Editors' Suggestion

Thickness-dependent electronic transport through epitaxial nontrivial Bi quantum films

Doaa Abdelbarey ,* Julian Koch, Zamin Mamiyev , Christoph Tegenkamp ,† and Herbert Pfnür ‡
Institut für Festkörperphysik, Leibniz Universität Hannover, Appelstraße 2, 30167 Hannover, Germany

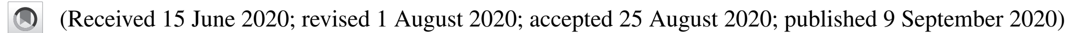
(Received 15 June 2020; revised 1 August 2020; accepted 25 August 2020; published 9 September 2020)

The magnetoconductance of Bi films grown epitaxially on Si(111) for a film thickness between 10 and 100 bilayers (BL) was investigated at a temperature of $T = 9$ K in magnetic fields up to 4 T oriented perpendicular to the surface plane. The thickness dependence of magnetoconductance (MC) and Hall resistivity was investigated in order to derive thickness dependent charge carrier concentrations as well as their mobilities and to identify corrections by weak antilocalization (WAL) to magnetoconductance. While the electronic transport in ultrathin films up to 30 bilayers (BL) turned out to take place mainly within the surface states, contributions of (bulk derived) quantum well states mix in at larger thicknesses and dominate incoherent transport above 70 BL. On the contrary, for the WAL contribution at magnetic fields normal to the surface, scattering within the surface states dominates at all thicknesses, as evident from the gradual change from values of $\alpha = -0.35$ to $\alpha = -1$ as a function of thickness. This finding reflects the decrease of coupling between the two interfaces going from a single combined conduction channel to two independent channels at the highest film thickness. Quick changes of both parts of magnetoconductance as a function of film thickness at the thinnest films seem to be strain induced by the Bi/Si interface. These results will advance the understanding of the transport properties of Bi thin films and reveal exotic quantum phenomena.

DOI: 10.1103/PhysRevB.102.115409

I. INTRODUCTION

Bismuth (Bi) is a comprehensively studied semimetal mainly because of its unusual electronic properties. These properties include the highly anisotropic Fermi surface, low carrier density, small effective mass, and long mean free path [1]. Furthermore, it has the highest resistivity as well as highest Hall coefficient among all metals. These properties make Bi films very attractive for spintronic devices [2] and indispensable to study its classical and quantum size effect (QSE) [3]. The ultrathin Bi(111) films are topologically nontrivial [4] and the surface of Bi films has a crucial influence on any device operation [5,6].

The electronic properties of Bi(111) surfaces and films were investigated intensively by angle-resolved photoemission spectroscopy (ARPES) [7–10]. Using first principles calculations, ARPES, and scanning tunneling spectroscopy (STS), the surface states turned out to be metallic and spin polarized due to the Rashba effect [8,11,12]. Furthermore, the metallic surface states dominate the transport when the film thickness is around several atomic layers and the quantum well states contribute little to the electronic structure near the Fermi level [9]. Moreover, Yang *et al.* [13] indicated that the topological edge states in ultrathin Bi films behave like in a two-dimensional topological insulator. Scanning tunneling microscopy (STM) investigations by Feldman *et al.* [14] show that these states represent a nematic quantum Hall liquid. This finding was confirmed by Randeria *et al.* [15] recently.

Based on the mesoscopic Fermi wavelength and the strong spin-orbit coupling in Bi films, there is a clear entanglement between topology, surface states, and quantum well states (QWS) for this material class. Therefore, the strict separation into surface and bulk states is inappropriate for the Bi quantum films. Latest high resolution ARPES experiments showed that the two spin-split surface bands, SS1 and SS2, bridge the $\overline{\Gamma}$ and $\overline{M}$ points [16]. Thereby, the connection of these states with valence and conduction bands, formally originating from the bulk, at the $\overline{M}$ point results in the formation of a nontrivial quantum film. Moreover, the variation of the film thickness comes along with a pronounced shift of the QWS. Thus the density of states (DOS) at the Fermi level, originating either from surface or quantized bulk bands, depends crucially on the film thickness. While the dispersion of the energetically low-lying SS2 surface state, which gives rise to hole pockets at E_F, is very similar to the dispersion of the valence band QWS, the SS1 state can give rise to an additional electron pocket close to the $\overline{M}$ point. In general, the decay lengths of the surface and interface states towards the bulk increase with larger momentum. Therefore, the localization of the transport channels for the charge carriers within the film change. This interplay of hybridized surface and quantum well states is altered for extremely thin films, leading to a deformation of quantum confinement potential via many-body electronic correlations. Very recently it has been suggested that this deformation modulates spatial distributions of quantized wave functions [17]. Moreover, the changes

*abdelbarey@fkp.uni-hannover.de
†Present address: Institut für Physik, Technische Universität Chemnitz, Reichenhainer Str. 70, D-09126 Chemnitz, Germany.
‡pfnuer@fkp.uni-hannover.de; Also at: Laboratory of Nano and Quantum Engineering (LNQE), Leibniz Universität Hannover, Schneiderberg 39, D-30167 Hannover, Germany.

 ©2020 American Physical Society

to the structure have a direct impact on transport [6]. Nevertheless, there is still a lack of a direct electronic transport experiments.

Over the past years, several magnetotransport measurements have been reported in UHV for Bi films that give evidence for significant surface contributions to the conductance [18–22]. Even at room temperature, the conductance of ultrathin Bi(111) films revealed a large ($\approx 1.5 \times 10^{-3}\ \Omega^{-1}$) surface conductivity [21,23]. For a film thickness of up to 25 BL, it was postulated that the metallic surface states dominate the transport [18,20,21], which is somewhat at variance with the claim that for films thicker than 20 BL the bulk derived QWS dominate the conductance [22].

An important and unavoidable imperfection for supported ultrathin films is the interface to the substrate. Together with the interface to vacuum, both interfaces establish the boundary condition for the quantum states and can form localized states at the Fermi level [23]. Since there is considerable mismatch between Si and Bi at the interface, residual strain and crystalline order can be strongly influenced by the inner interface—and thus by film preparation techniques [24]—and/or impurities, which in an extreme case can even change the topological properties of ultrathin Bi films [25,26]. For these reasons, it is highly desirable to prepare Bi films of high quality. Therefore, we used molecular beam epitaxy (MBE) to grow high quality defect-free layer-by-layer epitaxial films by selecting suitable growth conditions [27,28].

The combination of measurements of Hall resistivity and magnetoconductance allows us to validate scenarios where a change of sign of the dominant carrier contribution happens with increasing film thickness, when there is a major contribution of the quantized bulk states to conductance [24]. To the best of our knowledge, no comprehensive studies have been performed on the Hall resistivity, which give more insight into the contribution of metallic surface states and of their conductivity. To address this issue, we have investigated the thickness dependences of Hall resistivity, DC, and magnetoconductance in order to separate incoherent charge carrier scattering from coherent scattering. The latter leads to weak antilocalization (WAL). We derive mobilities, and charge carrier concentrations for electrons and holes, which demonstrate that there is strong coupling between the surface and quantized bulk states (QWS). Furthermore, we demonstrate that incoherent metallic transport starts to be dominated by contributions from these QWS at a critical thickness between 60 and 70 BL, while for WAL the surface states still play the major role for a magnetic field normal to the surface.

II. EXPERIMENTAL DETAILS

The transport measurements were performed on Bi films grown on low-doped Si(111) substrate ($\rho > 1000\ \Omega\,\mathrm{cm}$) of $15 \times 15 \times 0.5\ \mathrm{mm}^3$ size. The preparation of the substrate as well as the measurements were carried out in an ultrahigh vacuum system at a base pressure of 7×10^{-11} mbar. In order to avoid crosstalk between the eight electrical $TiSi_2$ contacts for transport measurements, four slits were machined into the substrate. Using standard procedures, the substrate was chemically cleaned and mounted on the sample holder. The final *in situ* cleaning step was performed by rapid annealing of the substrate using direct resistive heating for a few seconds at around 1050 °C. In addition to the removal of the oxide protection layer, this rapid high temperature annealing step also leads to the formation of a long-range ordered Si(111) 7×7 reconstruction. Details on contact fabrication and the cleaning procedures are further described in Ref. [29]. We are also aware of the fact that by the *in situ* high temperature annealing procedure the near-surface doping of the Si substrate can be affected [30]. While we tried to minimize this effect by keeping the pressure below 6×10^{-10} mbar even at the highest temperatures, this parasitic contribution of the space-charge layer turned out to be negligible at temperature below 100 K.

Molecular beam epitaxy was used to grow Bi films at 200 K followed by annealing to 410 K for several minutes; this ensures the growth of high quality crystalline Bi films. Layer thickness of Bi films is denoted as bilayers ($\mathrm{BL} = 1.14 \times 10^{15}\ \mathrm{atoms/cm^2}$). Furthermore, Bi was evaporated from a Knudsen cell using a ceramic crucible. The amounts were controlled by a quartz microbalance and typical deposition rates were around 1 BL per minute. The Bi coverage was calibrated by means of the $\sqrt{3} \times \sqrt{3}$ reconstructions on Si(111) and by recording bilayer oscillations in conductance during evaporation.

The morphologies of the Si substrate and the epitaxial films were checked by low energy electron diffraction (LEED). The transport setup allows us to measure the conductance G as a function of coverage as well as of temperature down to 9 K. This temperature was determined by using a diode on a dummy sample. Temperatures between 8.5 and 9 K were also determined from an extrapolation of the coherence length (l_Φ) curve according to Aitani *et al.* [22].

III. RESULTS AND DISCUSSION

A. Thickness-dependent magnetotransport

In order to examine the transport properties in Bi thin films, the magnetoconductance (MC) in a magnetic field perpendicular to the surface was determined for different thicknesses of the Bi film ranging from 10 BL to 100 BL. Before the transport measurements, the film quality was controlled by LEED, as exemplarily shown for a 20 BL film in Fig. 1(f). In agreement with previous publications [18,31], the Bi films are highly crystalline and oriented parallel to the main axes of the underlying Si(111) substrate. Figure 1(a) displays the changes in conductance induced by the magnetic field normal to the surface at 9 K. A negative magnetoconductance is observed for all thicknesses (10–100 BL). As seen from the change in shape as a function of thickness, there are at least two contributions to these curves, which we identify as being due to coherent and incoherent (diffuse, classical) contributions to magnetoconductance. The former is identical to the quantum correction leading to weak antilocalization (WAL). In fact, all measured MC curves can be accurately modeled considering these two contributions. Even for the thinnest film (10 BL), there is a small contribution of incoherent scattering. The incoherent contribution increases as a function of film thickness and this classical part dominates the MC for films thicker than 60 BL.

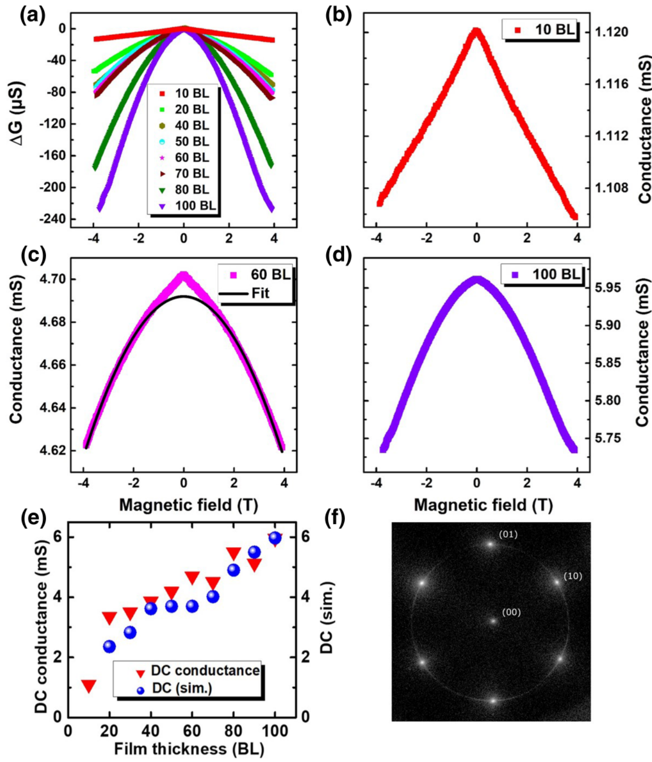

FIG. 1. Thickness dependence of magnetoconductance at 9 K. (a) Summary in the thickness range between 10 and 100 BL. Separate graphs at 10 BL (b), 60 BL (c), and 100 BL films (d), illustrating the changes of shape as a function of thickness. The blue dashed line in (c) represents a characteristic fit of the incoherent (diffuse) contribution. (e) Thickness dependence of conductance at zero magnetic field (triangles) together with calculated values (balls) obtained from best fits of carrier concentrations and mobilities derived from Hall resistances and diffuse magnetoconductance (see text). (f) LEED pattern of a 20 BL thick and annealed Bi film (beam energy = 78 eV) with the central (00) and first order diffraction spots.

We begin our analysis with the identification of the classical incoherent magnetoresistance contribution of thin Bi films using the two-carrier model and the separation of WAL and Drude background contributions, as described in our previous studies [18,19]. Furthermore, we measured also the Hall effect and DC conductance at 9 K for each layer thickness [see Fig. 1(e)]. These data sets were then fitted simultaneously in order to determine carrier concentrations of electrons and holes as well as their mobilities, i.e., one parameter set must fit the classical part of MC, Hall effect, and DC conductance. Figure 1(e) shows both the experimental data and those from best fits to Hall and DC conductance data. According to Ref. [32], using a two-band model, and under the assumption of diffuse scattering, the conductance G as a function of the magnetic field B reads:

$$G(B) = G(0)\frac{1 + (1-c)^2 \frac{\mu_n^2 \mu_p^2}{(\mu_n + c\mu_p)^2} B^2}{1 + \mu_n \mu_p \frac{\mu_p + c\mu_n}{\mu_n + c\mu_p} B^2}, \quad (1)$$

where $c \equiv p/n$ denotes the ratio of the hole and electron concentrations and $\mu_{n,p}$ are the averaged charge carrier mobilities of electrons and holes, respectively.

Interestingly, MC for the 10 BL film shows a cusplike feature near $B = 0\,\mathrm{T}$ and a nearly linear dependence with increasing field, as shown in Fig. 1(b). This form is typical for the coherent contribution to MC, which is dominated here by weak antilocalization (WAL) [33].

The same linear dependence with high magnetic fields has been observed on Bi thin films by Yin *et al.* [27,34]. However, for the growth conditions used in our study, such a peculiar situation was not found for higher thicknesses.

Furthermore, conductance is changed only by about 1% of the total conductance by the B field at this thickness. The sensitivity to B increases with layer thickness to roughly 3.5% at 100 BL. Given the total increase of conductance, most of this increased sensitivity is due to diffuse scattering.

This is evident from Fig. 1(c), which shows that by increasing the thickness to 60 BL, the cusp is still present—in fact, its amplitude even increases—but the curve loses its linear dependence and evolves into a more parabolic shape. This parabolic dependence at small B field is typical for diffuse scattering in magnetoconductance due to the Lorentz deflection [28,35–38], which is even more pronounced at 100 BL [Fig. 1(d)]. Due to this increase of the classical part with film thickness, the weak antilocalization becomes harder to be observed [37].

The total conductance at zero B field, shown in Fig. 1(e), increases sublinearly from 3 to 6 mS between 20 and 100 BL, but for the thinnest films we note the very high sensitivity to the exact preparation conditions, which play a crucial role for the quality of the interface. Thus a variation of σ_{total} up to a factor of 2 can be obtained in this range of thickness. The best annealed films of 10 and 20 BL [LEED pattern: See Fig. 1(f)] had the smallest conductance. As we will show below, strain effects of Bi/Si are important, influencing conductance for thin layers, and may explain the variation of absolute values in literature. Nevertheless, between 20 and 100 BL we used this total conductance as an additional quantity to be consistently fitted with the carrier concentrations and mobilities derived from Hall effect and magnetoconductance, as also shown in Fig. 1(e).

Summarizing this part, in the magnetic field dependence of conductance we identified two contributions: The incoherent (classical) part dominates at 80–100 BL. For thicknesses between 10 and 70 BL both contributions from the coherent quantum correction (WAL) and incoherent scattering were identified with an increasing weight of the classical part with increasing film thickness.

1. Hall resistivity

We now turn to the Hall measurements. The overall dependence of the Hall resistivity (i.e., the Hall sheet resistance) $\rho_H = U_H/I$ (with the Hall voltage U_H and measurement current I) on the magnetic field for different layer thicknesses (20–100 BL) is shown in Fig. 2(a). In order to separate any fraction of the longitudinal resistance from the Hall voltage, we swept the magnetic field between positive and negative values.

For film thicknesses between 20 and 60 BL the slope is negative but decreases until it changes sign between 60 and

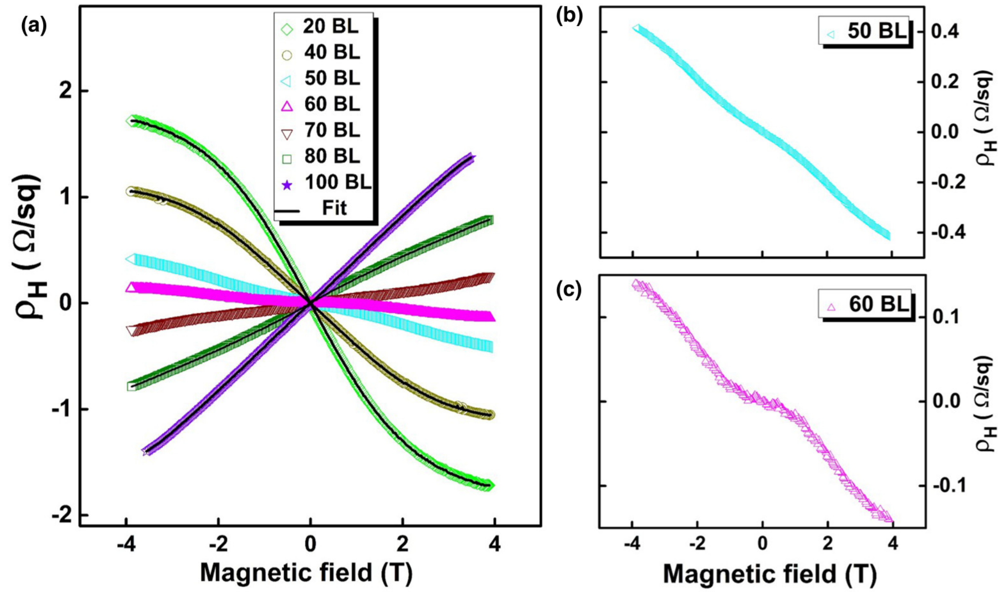

FIG. 2. Hall resistivity as a function of the magnetic field for Bi(111) films with various thicknesses. With increasing thickness, the slope of the Hall resistivity shifts from negative to positive. The Hall resistivity for 50 BL (b) and 60 BL (c) exhibit an unusual behavior at $B = 0$ T. The black solid lines represent the fitted curves using Eq. (2).

70 BL. The now positive slope increases for thicknesses from 70 to 100 BL.

Within the two-band model mentioned above, the Hall resistivity $\rho_H(B)$ for isotropic films depends on carrier concentration n, ratio $c = p/n$, carrier mobilities $\mu_{n,p}$, and magnetic field B, as follows [32]:

$$\rho_H(B) = -\frac{B}{ne}\frac{\mu_n^2 - c\mu_p^2 + (1-c)\mu_n^2\mu_p^2B^2}{(\mu_n + c\mu_p)^2 + (1-c)^2\mu_n^2\mu_p^2B^2}. \quad (2)$$

Exemplarily, for some data sets in Fig. 2(a) the accuracy of the modeling is demonstrated by a solid line. Although the slope is negative for the films from 20 to 60 BL, a consistent fit is only possible for $c > 1$ and the condition that $\mu_n^2/\mu_p^2 > c$ holds. Only with this condition, apart from the linear slopes, also the curvatures in these curves can be fitted properly. In other words, the majority of carriers are holes in this range of thickness, whereas the electron mobilities are larger than those of holes. Our results published previously [19] agree qualitatively but also demonstrate the importance of the detailed growth and annealing conditions since these determine the size of the crystals and effects of strain.

In the regime of thick films, i.e., 70–100 BL, the slope of the Hall resistivity notably changes sign and becomes positive, but also the curvature at higher B field changes sign. Therefore, the situation is now reversed compared to thin layers, i.e., there is a majority of electrons as carriers but also mobilities that are smaller than those of holes, as will be shown in the next section.

For Bi(111) films of intermediate thickness, the Hall resistivity curves exhibit an additional small modulation. As an example, Fig. 2(b) shows the Hall resistivity for a 50 BL film. The slope is still negative, and the almost linear overall slope demonstrates that the system is getting close to $c = 1$. The nonlinearity in ρ_H at low B fields, however, cannot be described within the two-band model of Eq. (2). It is even more pronounced in the curve for 60 BL [see Fig. 2(c)]. Its appearance suggests the presence of more than two bands, as observed in other Bi-based topological systems [39,40]. Such nonlinearities in the Hall resistivity have been attributed to the coexistence of bulk (quantum well) and surface transport channels previously [41,42]. This close entanglement of surface and quantum well states due to the topological properties of the Bi(111) film [17] will become clearer when looking at the charge carrier mobilities and concentrations in more detail.

2. *Charge carrier mobilities and concentrations*

Figure 3 shows the charge carrier mobilities obtained from the classical magnetoresistance fit in conjunction with the Hall curves for both carrier types. For 20–60 BL films, the electron mobilities are higher than hole mobilities. Conversely,

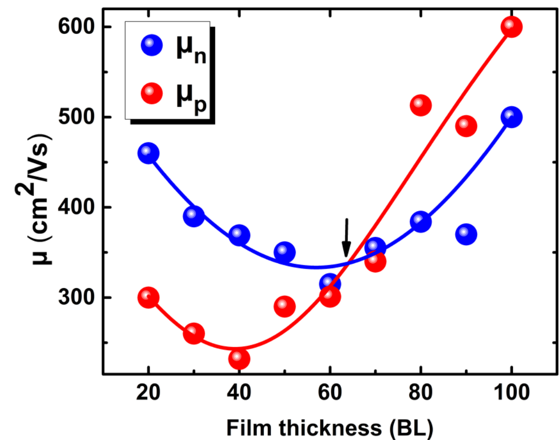

FIG. 3. Film thickness dependence of charge carrier mobilities at 9 K of electrons (blue) and holes (red). The lines are just guides to the eye.

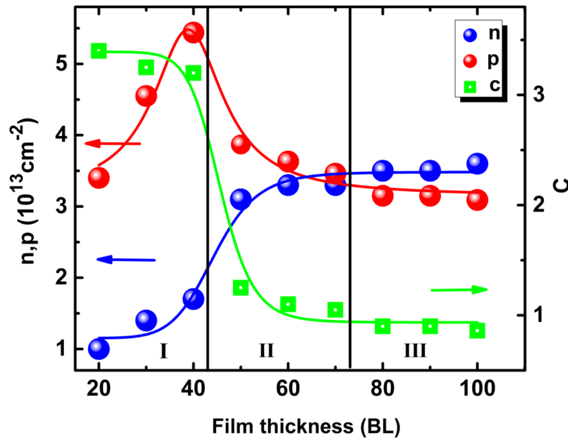

FIG. 4. Electron (n, blue balls) and hole (p, red balls) concentrations, together with their ratio $c = p/n$ (green squares) as a function of the film thickness as extracted from fits according to Eqs. (1) and (2). Three ranges marked by two vertical lines can be identified (see text). The colored lines are just guides to the eye.

the hole mobilities turn out to be larger than the electron mobilities for thicker films of 80–100 BL. Hence, there is a crossover in the range of 60–70 BL.

From our analysis of Hall, MC, and DC data, we also extracted the charge carrier concentrations. We plot the extracted carrier concentrations, p and n, and their ratio c as a function of the film thickness in Fig. 4. Three different thickness regimes can be distinguished.

In region I ($20 \leqslant d \leqslant 40$ BL), the concentrations of both electrons and holes increase as a function of layer thickness by approximately the same factor. For 40 BL films, the magnitude of carrier concentrations for electrons and holes is 1.8×10^{13} cm^{-2} and 5.5×10^{13} cm^{-2}, respectively, i.e., conductance in this range of thickness is strongly dominated by holes.

Region II ($40 < d < 70$ BL) is characterized by a decrease of hole concentration whereas the electron (n) concentration still increases so that the overall carrier concentration is approximately constant. As a consequence DC conductance changes little in this range of thickness. A crossover occurs at 60 to 70 BL, where both reach the same value of approximately 3.3×10^{13} cm^{-2}.

The last region ($80 \leqslant d \leqslant 100$ BL) of Fig. 4 shows no significant changes to the carrier concentrations. The electron concentration is now higher than that of holes with nearly constant values of 3.5×10^{13} cm^{-2} and 3.1×10^{13} cm^{-2}, respectively.

a. Discussion of charge carrier concentrations. These results can nicely be interpreted and compared with data from photoemission [7,16,17,43] and with recent DFT simulations [17,44,45]. Indeed, according to ARPES [16] combined with theoretical calculations, an anomalous thickness evolution of quantum well state subbands (QWSs) at the $\overline{\Gamma}$ point was recently confirmed [17], which turned out to be particularly relevant for thin layers in the range of region I. In this region, the trends of carrier concentrations derived from our measurements follow closely those observed both in ARPES experiments. They corroborate the dominance of p carriers in this range of thickness, mainly caused by partially occupied surface states, also demonstrate an intriguing interplay between surface and quantum well states.

The increase in hole concentration to a maximum at 40 BL seems to be peculiar and may be an indication of particularly strong hybridization of these states in this range of thickness. Changes of band structure as a function of film thickness can also cause charge redistribution due to different relative occupation of quantum well and surface states close to the Fermi level [7,11,16,17,46]. This allows for dynamic charge transfer between the surface and quantum well states [47]. Apparently, such a mechanism is the reason for the observed decrease of hole concentration in the surface state above 40 BL. Such hybridizations are not included in our two-band model used for the fits. Therefore, they can only be considered as effective charge concentrations. Also an influence by strain on the effective carrier densities for the thinnest Bi layers investigated, seen in simulations [17], cannot be excluded, but is hard to quantify.

The strong increase of electron concentration, starting at around 30 BL, can directly be explained from the thickness dependent decrease in energetic position of a QWS with a high DOS close to the $\overline{M}$ point, coupled with a reduced spacing of the QWS. While it is totally unoccupied at small thickness, it crosses the Fermi level at larger thickness. This happens at a critical thickness between 30 and 40 BL [45], in good agreement with the observed strong increase of n in this range (see Fig. 4). Since this state overlaps energetically also with the surface states, diffuse scattering allows exchange between these states and the opening of new channels of conductance. Moreover, the overlap of surface states with the QWS close to the $\overline{M}$ point, starting at this layer thickness, forms a surface resonance state [7,11,16,46]. The dynamic charge transfer between these states makes the strict separation into surface and bulk-derived states obsolete [47].

Furthermore, according to simulations [17], this partially occupied quantum well state has a relatively high effective mass. Therefore, with the increasing contribution of this state to the conducting electron density it is not surprising that the average electron mobility gets reduced up to 60 BL relative to thinner Bi films.

From this agreement with calculations we also conclude that the contribution of this QWS to the electron charge carrier density starts to dominate above 70 BL. Indeed, for films $\geqslant$60 BL, the charge carrier densities of electrons and holes and their ratio become independent of thickness.

Looking at the variation of the charge carrier concentration in the whole range of d investigated here, we see that it is mainly the variation of the electron concentration that contributes to changes in conductance, while the changes in hole concentration as a function of layer thickness, mostly caused by relaxations and hybridizations of the surface states, remain comparatively small. The electron concentration more than triples between 20 and 70 BL from 1×10^{13} cm^{-2} to 3.5×10^{13} cm^{-2} (see Fig. 4). This increase is mainly caused by the partial occupation of the quantum well state that hybridizes with the surface states around the $\overline{M}$ point. Thus there is a considerable admixture of quantum well contributions to the pure surface state conductance for electrons. For films with

$d \geqslant 80$ BL, the transport is dominated by the quantized bulk states rather than by the surfaces (region III of Fig. 4).

In principle, also contributions to conductance from the QWS that cross the Fermi level close to the Γ point [44] have to be taken into account. Their number is also increasing with layer thickness. However, from the comparison with simulated band structure data [17,44] we conclude that the variations of the electron pocket close to $\bar{\Gamma}$ as a function of d have only a small effect to the overall carrier concentration due to its low density of states, so that mainly the electron pocket close to the $\overline{M}$ point and its variation as a function of d is crucial in our context.

Concluding the discussion of the variation of charge carrier concentrations as a function of film thickness, we demonstrated that films with $20 \leqslant d \leqslant 70$ show an intriguing entanglement between the surface and quantum well states. With increasing thickness the contribution of the quantum well state to the charge carrier concentration increases and become the main contributor for $d \geqslant 80$ BL.

b. Discussion of mobilities. We now turn to the interpretation and discussion of mobilities, whose dependence on d (see Fig. 3) reveals further interesting properties. We first want to point out that the change of their ratio μ_p/μ_n from >1 to ⊲ at 60 BL is clearly correlated with the sign change of the Hall resistivity. This crossover close to 60–70 BL is coupled with the general *increase* of the charge carrier mobilities with increasing thickness. This finding is fully compatible with the assumption from above that with increasing thickness, in addition to surface state dominated transport, there is now a large contribution to conductance by a QWS of mainly electron character, which is extended throughout the whole film. The qualitatively same dependence of electron and hole mobilities on film thickness is a further argument for intermixing surface and quantum well states, but the steeper increase of hole mobility indicates a stronger weight of surface scattering for the holes. The latter behavior is expected, since the Lorentz force acts in plane for a B field normal to the surface, so that the B dependence of conductance strongly weights scattering processes within the surface plane [48].

Going one step further, the linear increase of scattering lengths as a function of d not only indicates the strong contributions of QWS, it must also mean that even for the thick layers interface scattering still dominates. Indeed a linear extrapolation of mobilities above 60 BL to film thickness zero leads to zero electron mobility within error bars, pointing in the same direction.

Also at small thickness, both types of carriers show a common trend of decrease of mobility for d up to 40 BL. Here stress relaxation mechanisms at the Bi/Si interface may come into play [49,50], as indicated by the differences between the Bi/Ge(111) and the Bi/Si(111) system [17]. On the other hand, also the continuously changing hybridization between surface states and QWS as a function of d may play a role for this observation. This makes it difficult to identify the origin of the observed decrease of mobilities in more detail.

B. Quantum correction to the magnetoconductance

In addition to the dominant classical magnetoconductance signal, the films show cusplike features at low fields (cf. Fig. 1). For Bi [18,52] as well as Bi-based compounds [53,54], the sharp cusp near the zero field has often been observed. It can be attributed to the weak antilocalization (WAL) effect and reflects the strong spin-orbit coupling in Bi (111) surface states [55].

The change in conductance $\Delta G(B) = G(B) - G(0)$ as a function of the perpendicular magnetic field can be modeled within the framework of the Hikami-Larkin-Nagaoka (HLN) theory [51] as follows:

$$\Delta G(B_\perp) = \alpha \frac{e^2}{2\pi^2\hbar}\left[\Psi\left(\frac{1}{2} + \frac{\hbar}{2eB_\perp l_\Phi^2}\right) - ln\left(\frac{\hbar}{4eB_\perp l_\Phi^2}\right)\right]. \tag{3}$$

The dependence on magnetic field $B_\perp$ normal to the surface is described by the di-gamma function, Ψ, in which l_Φ denotes the phase coherence length. The prefactor α represents a coefficient indicating the type of localization. In case of WAL, $\alpha = -0.5$ is expected for each transport channel that either carries a π Berry phase [56] or bears a strong spin-orbit interaction. Using the prefactor α and phase coherence length l_Φ as fitting parameters, the curves of the variation of magnetoconductance ΔG measured in perpendicular magnetic field (at 9 K) can be reasonably well fitted to the Hikami-Larkin-Nagaoka [51] model, as shown in Fig. 5(a). The fitting results of α and l_Φ are displayed in Figs. 5(b) and 5(c) as a function of film thickness.

The coherence length l_Φ was found to be essentially independent of the thickness of the layers and has a value of about 60 nm. This is a clear indicator of the high quality of the films. Furthermore, the thickness of all films up to 70 BL (=28 nm) are smaller than $l_\phi/2$, i.e., coherent scattering paths involving both surfaces are possible only for thinner layers. On the other hand, the thickness d is not limiting the coherent scattering length for the thin films, so that for these films such coherent scattering processes between the two interfaces involving both surface and quantum well states have to be taken into account [22,57]. This interplay between the different states leads to a deviation of α from -0.5 with increasing film thickness [58].

The α derived from our fits was found to vary strongly with film thickness. While for the 10 BL film a value of $\alpha = -0.35$ was found, which is in agreement with that of Aitani *et al.*, [22] it changes to a nearly constant value slightly close to -0.6 between 20 and 40 BL, as shown in Fig. 5(b). From 50 BL on, there is a gradual decrease in α starting at -0.66 for 50 BL and reaching -0.8 for the 70 BL film. For the thickest films, i.e., 80–100 BL, α is close to -1, which coincides with the value for two independent parallel conductive channels each with a contribution of -0.5 within HLN theory.

The negative value of α indicates the dominance of spin-dependent scattering within the strongly spin-polarized bands, as mentioned. The lack of inversion symmetry in these ultrathin quantum films leads to strong spin-orbit splitting for Bi that is mainly concentrated at the surface due to the Rashba effect so that mainly the surface states are spin split, as indeed found for this system [17].

The value of $\alpha = -0.6$ already deviates from the description that coherent scattering happens within one single

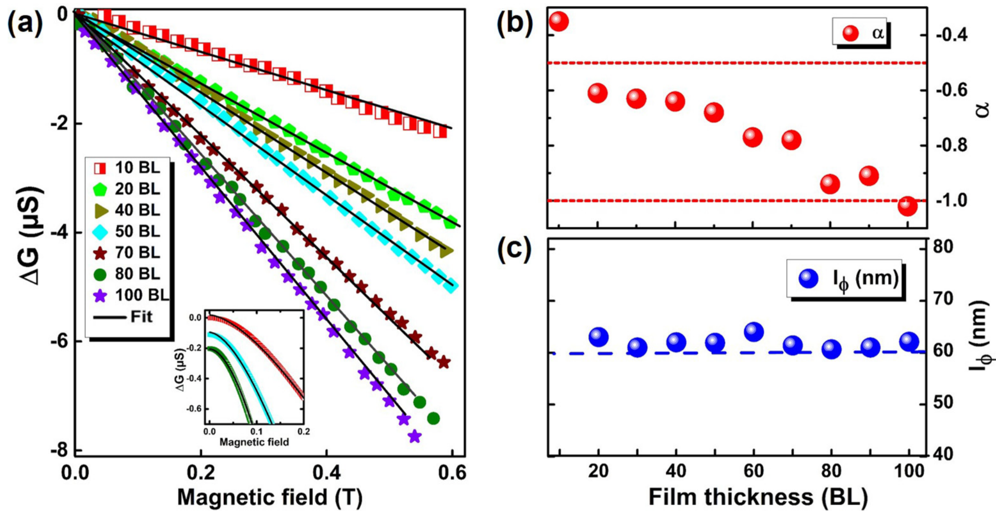

FIG. 5. Coherent contribution of magnetoconductance from Fig. 1 described by WAL. The Hikami-Larkin-Nagaoka (HLN) [51] fit of the change in conductance at low magnetic field for Bi 10 to 100 BL is shown in (a). Inset: Magnification of the 10, 50, and 80 BL curves close to the origin. 50 and 80 BL curves are offset by -0.1 μS. (b) Amplitude α and (c) phase coherence length l_Φ as a function of layer thickness.

channel provided by the spin polarized surface states [7,17,44] that are strongly coupled between top and bottom [26]. Indeed, as already discussed above, there is close entanglement between surface and quantum well states, of which a varying number $\gg 1$ is crossing the Fermi level at all thicknesses investigated here. Such hybridized states have been identified both in experiment [7,16,17,43] and in theory [17,44]. Since the hybridization between (bulk) quantum well and surface states is characteristic for all thicknesses of Bi films investigated here, values of α deviating from half-integer values must be expected. Taking this argument seriously, even a half-integer value of $\alpha = -0.5$ must be considered as an effective value [59], i.e., coherent scattering for closed paths within the surface plane appears as spin-dominated scattering in an effective single channel resulting from strong coupling of the hybridized surface states.

Furthermore, in these ultrathin films a residual distortion by compressive stress due to mismatch with the substrate may still play a role, as suggested in Ref. [17], that modifies energetic positions of both quantum well and surface states and their dispersion. The quick change of α between 10 and 20 BL to a nearly constant value at higher layer thickness points into this direction.

This point of view fits nicely to the gradual change of α as a function of d, seen in Fig. 5(b), that reaches the value of $\alpha = -1$ close to 100 BL and forms a second plateau close to this value at and above 80 BL. While formally the gradual decrease of α as a function of d can be described by the reduction of coupling between the two surfaces [55,60–62], it is, in view of the contributions from the QWS to conductance discussed above, not obvious that the limiting case for coherent scattering for thick films is at $\alpha = -1$, i.e., at the value of two effectively independent and strongly spin polarized channels [28,63,64].

Taking into account that only the surface states are strongly spin polarized, and that for thick films there is only one surface state per interface, $\alpha = -1$ turns out to be in fact the smallest possible value for two independent conducting surface channels. Contributions from unpolarized bands exhibiting only weak localization (WL) should make this value more positive. This means that there can only be minor contributions from WL, expected from the mainly unpolarized quantum well states, which in principle may compete with WAL [65]. A possible reason for this finding may be that the B field normal to the surface strongly weights phase conserving scattering paths within the surface plane that generate magnetic flux. This suggestion is further supported by the finding (see Sec. III A 2) that interface scattering dominates at all film thicknesses, although explicitly tested only for incoherent scattering. Therefore, charge carriers within QWS scattered once at the surface need to be scattered back within the film without reaching the other interface for the thicker films investigated due to the limited coherence length. This is obviously an unlikely process. Together with the weight given by the orientation of the B field, coherent scattering is much more likely within surface states than in QWS that are extended throughout the whole film.

IV. CONCLUSIONS

The detailed magnetotransport data shown in this paper on Bi quantum films give insight into the transport properties of these films. By a systematic investigation of magnetoconductance in a magnetic field oriented normal to the film surface and Hall resistivity for a layer thickness between 10 and 100 BL, we were able to determine contributions to conductance by incoherent scattering, characterized by carrier concentrations, and mobilities, and by coherent scattering described by α and l_Φ. We demonstrate an intriguing interplay between surface and quantum well states, which for the ultrathin films even hybridize due to the symmetry break normal to the film surface [17].

Furthermore, adsorption on a substrate—Si(111) in our case—most likely leads for the ultrathin films to slightly strained Bi layers. This strain seems to contribute to the quick changes of carrier concentrations and of α as a function of

layer thickness in the range up to 40 BL. Whether these changes induce a topologically nontrivial signature cannot be decided on the basis of magnetotransport alone.

The admixture of bulk-derived quantum well states with n character at film thicknesses above 40 BL leads to sign reversal in the Hall resistivity at a critical film thickness of 60 to 70 BL, to an anomalous behavior in mobility and to a further increase of conductance. We hope that these results add to a clarification of the long-standing controversy of relative "surface" and "bulk" contributions to conductance. While the entanglement of surface and quantum well states does not allow a separation of their contributions in a strict sense, it should have become clear from this investigation that both parts are important with a dominance of the contribution of the surface states for the ultrathin films at a thickness below 40 BL.

In contrast, for coherent scattering (WAL), under the chosen geometry with B normal to the surface, the contributions from bulk quantum well states appear to be small for all thicknesses investigated, i.e., these scattering processes happen within the surface states. The reduction of coupling between the two surfaces as a function of thickness is reflected in coherent scattering by the gradual change from $\alpha = -0.6$ at 20 BL to $\alpha = -1$ above 80 BL. These values are compatible with those expected for strong spin-orbit scattering in one and two conducting channels and could be interpreted as the result of gradual decoupling of the two interfaces as a function of layer thickness. This interpretation, however, may be too simple, since a varying number of conducting channels is involved as a function of thickness in this fully quantized system, as outlined above. Therefore, α values can only be considered as effective values.

ACKNOWLEDGMENTS

We would like to thank Dr. Suguru Ito for several fruitful discussions on his photoemission spectroscopy data. This work has been supported by the Deutsche Forschungsgemeinschaft through project Pf238/31.

[1] W. Ning, F. Kong, Y. Han, H. Du, J. Yang, M. Tian, and Y. Zhang, Sci. Rep. **4**, 7086 (2014).

[2] M. Jankowski, D. Kamiński, K. Vergeer, M. Mirolo, F. Carla, G. Rijnders, and T. R. J. Bollmann, Nanotechnology **28**, 155602 (2017).

[3] N. Marcano, S. Sangiao, C. Magén, L. Morellón, M. R. Ibarra, M. Plaza, L. Pérez, and J. M. De Teresa, Phys. Rev. B **82**, 125326 (2010).

[4] Y. Ohtsubo, L. Perfetti, M. O. Goerbig, P. L. Fèvre, F. Bertran, and A. Taleb-Ibrahimi, New J. Phys. **15**, 033041 (2013).

[5] M.-Y. Yao, F. Zhu, C. Q. Han, D. D. Guan, C. Liu, D. Qian, and J.-f. Jia, Sci. Rep. **6**, 21326 (2016).

[6] C. König, S. Fahy, and J. C. Greer, Phys. Rev. Mater. **3**, 065002 (2019).

[7] T. Hirahara, T. Nagao, I. Matsuda, G. Bihlmayer, E. V. Chulkov, Y. M. Koroteev, P. M. Echenique, M. Saito, and S. Hasegawa, Phys. Rev. Lett. **97**, 146803 (2006).

[8] T. Hirahara, K. Miyamoto, I. Matsuda, T. Kadono, A. Kimura, T. Nagao, G. Bihlmayer, E. V. Chulkov, S. Qiao, K. Shimada, H. Namatame, M. Taniguchi, and S. Hasegawa, Phys. Rev. B **76**, 153305 (2007).

[9] T. Hirahara, T. Nagao, I. Matsuda, G. Bihlmayer, E. V. Chulkov, Y. M. Koroteev, and S. Hasegawa, Phys. Rev. B **75**, 035422 (2007).

[10] A. Takayama, T. Sato, S. Souma, and T. Takahashi, Phys. Rev. Lett. **106**, 166401 (2011).

[11] Y. M. Koroteev, G. Bihlmayer, J. E. Gayone, E. V. Chulkov, S. Blügel, P. M. Echenique, and P. Hofmann, Phys. Rev. Lett. **93**, 046403 (2004).

[12] J. I. Pascual, G. Bihlmayer, Y. M. Koroteev, H.-P. Rust, G. Ceballos, M. Hansmann, K. Horn, E. V. Chulkov, S. Blügel, P. M. Echenique, and P. Hofmann, Phys. Rev. Lett. **93**, 196802 (2004).

[13] F. Yang, L. Miao, Z. F. Wang, M.-Y. Yao, F. Zhu, Y. R. Song, M.-X. Wang, J.-P. Xu, A. V. Fedorov, Z. Sun, G. B. Zhang, C. Liu, F. Liu, D. Qian, C. L. Gao, and J.-F. Jia, Phys. Rev. Lett. **109**, 016801 (2012).

[14] B. E. Feldman, M. T. Randeria, A. Gyenis, F. Wu, H. Ji, R. J. Cava, A. H. MacDonald, and A. Yazdani, Science **354**, 316 (2016).

[15] M. T. Randeria, K. Agarwal, B. E. Feldman, H. Ding, H. Ji, R. J. Cava, S. L. Sondhi, S. A. Parameswaran, and A. Yazdani, Nature (London) **566**, 363 (2019).

[16] S. Ito, B. Feng, M. Arita, A. Takayama, R.-Y. Liu, T. Someya, W.-C. Chen, T. Iimori, H. Namatame, M. Taniguchi, C.-M. Cheng, S.-J. Tang, F. Komori, K. Kobayashi, T.-C. Chiang, and I. Matsuda, Phys. Rev. Lett. **117**, 236402 (2016).

[17] S. Ito, M. Arita, J. Haruyama, B. Feng, W.-C. Chen, H. Namatame, M. Taniguchi, C.-M. Cheng, G. Bian, S.-J. Tang, T.-C. Chiang, O. Sugino, F. Komori, and I. Matsuda, Sci. Adv. **6**, eaaz5015 (2020).

[18] D. Lükermann, S. Sologub, H. Pfnür, and C. Tegenkamp, Phys. Rev. B **83**, 245425 (2011).

[19] P. Kröger, D. Abdelbarey, M. Siemens, D. Lükermann, S. Sologub, H. Pfnür, and C. Tegenkamp, Phys. Rev. B **97**, 045403 (2018).

[20] N. Miyata, R. Hobara, H. Narita, T. Hirahara, S. Hasegawa, and I. Matsuda, Jpn. J. Appl. Phys. **50**, 036602 (2011).

[21] T. Hirahara, I. Matsuda, S. Yamazaki, N. Miyata, S. Hasegawa, and T. Nagao, Appl. Phys. Lett. **91**, 202106 (2007).

[22] M. Aitani, T. Hirahara, S. Ichinokura, M. Hanaduka, D. Shin, and S. Hasegawa, Phys. Rev. Lett. **113**, 206802 (2014).

[23] J. W. Wells, K. Handrup, J. F. Kallehauge, L. Gammelgaard, P. Bøggild, M. B. Balslev, J. E. Hansen, P. R. E. Petersen, and P. Hofmann, J. Appl. Phys. **104**, 053717 (2008).

[24] E. I. Rogacheva, S. N. Grigorov, O. N. Nashchekina, A. Yakovleva, and S. Lyubchenko, in *Twenty-First International Conference on Thermoelectrics, 2002. Proceedings ICT '02, Long Beach, CA, USA* (IEEE, 2002), pp. 284–287.

[25] I. Aguilera, C. Friedrich, and S. Blügel, Phys. Rev. B **91**, 125129 (2015).

[26] K. Zhu, L. Wu, X. Gong, S. Xiao, and X. Jin, Phys. Rev. B **94**, 121401(R) (2016).

[27] A. Roy, S. Guchhait, S. Sonde, R. Dey, T. Pramanik, A. Rai, H. Movva, L. Colombo, and S. Banerjee, Appl. Phys. Lett. **102**, 163118 (2013).
[28] L. Yang, Z. Wang, M. Li, X. P. A. Gao, and Z. Zhang, Nanoscale Adv. **1**, 2303 (2019).
[29] C. Tegenkamp, D. Lükermann, S. Akbari, M. Czubanowski, A. Schuster, and H. Pfnür, Phys. Rev. B **82**, 205413 (2010).
[30] F. Edler, I. Miccoli, H. Pfnür, and C. Tegenkamp, J. Phys.: Condens. Matter **31**, 214001 (2019).
[31] T. Nagao, J. T. Sadowski, M. Saito, S. Yaginuma, Y. Fujikawa, T. Kogure, T. Ohno, Y. Hasegawa, S. Hasegawa, and T. Sakurai, Phys. Rev. Lett. **93**, 105501 (2004).
[32] A. B. Pippard, *Magnetoresistance in Metals* (Cambridge University Press, Cambridge, UK, 1989).
[33] Y. F. Komnik, E. I. Bukhshtab, V. V. Andrievskii, and A. V. Butenko, J. Low Temp. Phys. **52**, 315 (1983).
[34] S.-L. Yin, X.-J. Liang, and H.-W. Zhao, Chin. Phys. Lett. **30**, 087305 (2013).
[35] T. Chen, Q. Chen, K. Schouteden, W. Huang, X. Wang, Z. Li, F. Miao, X. Wang, Z. Li, B. Zhao, S. Li, F. Song, J. Wang, B. Wang, C. Van Haesendonck, and G. Wang, Nat. Commun. **5**, 5022 (2014).
[36] M. Liu, C.-Z. Chang, Z. Zhang, Y. Zhang, W. Ruan, K. He, L.-l. Wang, X. Chen, J.-F. Jia, S.-C. Zhang, Q.-K. Xue, X. Ma, and Y. Wang, Phys. Rev. B **83**, 165440 (2011).
[37] N. Marcano, S. Sangiao, M. Plaza, L. Pérez, A. F. Pacheco, R. Córdoba, M. C. Sánchez, L. Morellón, M. R. Ibarra, and J. M. De Teresa, Appl. Phys. Lett. **96**, 082110 (2010).
[38] D. L. Mo, W. B. Wang, and Q. Cai, Nanoscale Res. Lett. **11**, 354 (2016).
[39] K. Shrestha, D. E. Graf, V. Marinova, B. Lorenz, and P. C. W. Chu, Philos. Mag. **97**, 1740 (2017).
[40] J. S. Kim, S. S. A. Seo, M. F. Chisholm, R. K. Kremer, H.-U. Habermeier, B. Keimer, and H. N. Lee, Phys. Rev. B **82**, 201407(R) (2010).
[41] Z. Ren, A. A. Taskin, S. Sasaki, K. Segawa, and Y. Ando, Phys. Rev. B **82**, 241306(R) (2010).
[42] P. Ngabonziza, Y. Wang, and A. Brinkman, Phys. Rev. Materials **2**, 044204 (2018).
[43] T. Hirahara, T. Shirai, T. Hajiri, M. Matsunami, K. Tanaka, S. Kimura, S. Hasegawa, and K. Kobayashi, Phys. Rev. Lett. **115**, 106803 (2015).
[44] G. Cantele and D. Ninno, Phys. Rev. Materials **1**, 014002 (2017).
[45] T.-R. Chang, Q. Lu, X. Wang, H. Lin, T. Miller, T.-C. Chiang, and G. Bian, Crystals **9**, 510 (2019).
[46] C. R. Ast and H. Höchst, Phys. Rev. Lett. **87**, 177602 (2001).
[47] E. Kneedler, D. Skelton, K. E. Smith, and S. D. Kevan, Phys. Rev. Lett. **64**, 3151 (1990).
[48] N. Bansal, Y. S. Kim, M. Brahlek, E. Edrey, and S. Oh, Phys. Rev. Lett. **109**, 116804 (2012).
[49] J. S. Speck, A. C. Daykin, A. Seifert, A. E. Romanov, and W. Pompe, J. Appl. Phys. **78**, 1696 (1995).
[50] S. H. Huang, G. Balakrishnan, A. Khoshakhlagh, A. Jallipalli, L. R. Dawson, and D. L. Huffaker, Appl. Phys. Lett. **88**, 131911 (2006).
[51] S. Hikami, A. I. Larkin, and Y. Nagaoka, Prog. Theor. Phys. **63**, 707 (1980).
[52] D. Lükermann, S. Sologub, H. Pfnür, C. Klein, M. Horn-von Hoegen, and C. Tegenkamp, Phys. Rev. B **86**, 195432 (2012).
[53] J. Chen, X. Y. He, K. H. Wu, Z. Q. Ji, L. Lu, J. R. Shi, J. H. Smet, and Y. Q. Li, Phys. Rev. B **83**, 241304(R) (2011).
[54] A. A. Taskin, S. Sasaki, K. Segawa, and Y. Ando, Phys. Rev. Lett. **109**, 066803 (2012).
[55] J. J. Cha, D. Kong, S.-S. Hong, J. G. Analytis, K. Lai, and Y. Cui, Nano Lett. **12**, 1107 (2012).
[56] T. Ando, T. Nakanishi, and R. Saito, J. Phys. Soc. Jpn. **67**, 2857 (1998).
[57] Y. Ando, J. Phys. Soc. Jpn. **82**, 102001 (2013).
[58] H. Steinberg, J.-B. Laloë, V. Fatemi, J. S. Moodera, and P. Jarillo-Herrero, Phys. Rev. B **84**, 233101 (2011).
[59] H. Tang, X. Yan, Y. Xiong, K. Dou, Y. Zhao, J. Jie, X. Wang, Q. Fu, J. Yang, M. Lu, and D. Xu, npj Quantum Materials **4**, 1 (2019).
[60] D. Kim, P. Syers, N. P. Butch, J. Paglione, and M. S. Fuhrer, Nat. Commun. **4**, 2040 (2013).
[61] L. Bao, L. He, N. Meyer, X. Kou, P. Zhang, Z.-g. Chen, A. V. Fedorov, J. Zou, T. M. Riedemann, T. A. Lograsso, K. L. Wang, G. Tuttle, and F. Xiu, Sci. Rep. **2**, 726 (2012).
[62] L.-X. Wang, Y. Yan, Z.-M. Liao, and D.-P. Yu, Appl. Phys. Lett. **106**, 063103 (2015).
[63] M. Lang, L. He, X. Kou, P. Upadhyaya, Y. Fan, H. Chu, Y. Jiang, J. H. Bardarson, W. Jiang, E. S. Choi, Y. Wang, N.-C. Yeh, J. Moore, and K. L. Wang, Nano Lett. **13**, 48 (2013).
[64] I. Garate and L. Glazman, Phys. Rev. B **86**, 035422 (2012).
[65] H.-Z. Lu and S.-Q. Shen, Phys. Rev. Lett. **112**, 146601 (2014).